Tracer tests in a fractured dolomite
2. Analysis of mass transfer in single-well injection-withdrawal tests

Roy Haggerty and Sean W. Fleming[1]

Department of Geosciences, Oregon State University, Corvallis, Oregon

Lucy C. Meigs and Sean A. McKenna

Geohydrology Department, Sandia National Laboratories, Albuquerque, New Mexico

Abstract. We investigated multiple-rate diffusion as a possible explanation for observed behavior in a suite of single-well injection-withdrawal (SWIW) tests conducted in a fractured dolomite. We first investigated the ability of a conventional double-porosity model and a multirate diffusion model to explain the data. This revealed that the multirate diffusion hypothesis/model is consistent with available data and is capable of matching all of the recovery curves. Second, we studied the sensitivity of the SWIW recovery curves to the distribution of diffusion rate coefficients and other parameters. We concluded that the SWIW test is very sensitive to the distribution of rate coefficients but is relatively insensitive to other flow and transport parameters such as advective porosity and dispersivity. Third, we examined the significance of the constant double-log late time slopes (−2.1 to −2.8), which are present in several data sets. The observed late time slopes are significantly different than would be predicted by either conventional double-porosity or single-porosity models and are believed to be a distinctive feature of multirate diffusion. Fourth, we found that the estimated distributions of diffusion rate coefficients are very broad, with the distributions spanning a range of up to 3.6 orders of magnitude. Fifth, when both heterogeneity and solute drift are present, late time behavior similar to multirate mass transfer can occur. Although it is clear that multirate diffusion occurs in the Culebra, the number of orders of magnitude of variability may be overestimated because of the combined effects of drift and heterogeneity.

1. Introduction

The first paper in this series [*Meigs and Beauheim*, this issue] describes the field setting, goals, design, implementation, and results of a suite of single-well injection-withdrawal (SWIW) and multiwell convergent-flow tracer experiments conducted in the Culebra Dolomite Member of the Rustler Formation at the Waste Isolation Pilot Plant (WIPP) site in southeastern New Mexico. The third paper in this series [*McKenna et al.*, this issue] examines a subset of the data from the multiwell convergent-flow tracer tests that were conducted at the same locations as the SWIW tests. McKenna et al. also compare results obtained from the two different types of test and discusses long-term transport implications. Further information, including the complete data sets, is given by *Meigs et al.* [2000].

The effects of multiple rates of mass transfer (or "multirate" mass transfer) have been theoretically predicted in the past and have also been observed in a number of laboratory experiments; these effects have not, until now, been documented at the field scale. In this paper, we investigate the multirate diffusion hypothesis as it relates to the SWIW tests. The hypoth-

esis postulates that a distribution of apparent diffusion coefficients and diffusion length scales is responsible for anomalous behavior (e.g., anomalously long tails and timescale-dependent rate coefficients) in many laboratory and field tracer experiments. As such, the goals of this investigation were to (1) investigate the hypothesis that multirate diffusion could be responsible for the observed recovery behavior in the Culebra SWIW tests; (2) develop a methodology for estimating the distribution of rate coefficients responsible for the observed behavior; (3) examine whether the hypothesis and resulting model are consistent with other hard and soft data; and (4) examine the significance of the late time slope of the observed SWIW recovery curves, a slope which is common to data collected from several well tests.

As a model of mass transfer, multirate diffusion invokes diffusion between an advection-dominated ("mobile") zone and a diffusion-dominated rock matrix ("immobile zone") that is heterogeneous at the pore scale. The multirate diffusion model [*Haggerty and Gorelick*, 1995, 1998] is essentially a modified double-porosity model [e.g., *Neretnieks*, 1980, 1993] (see also Figure 1 and section 3) consisting of advective porosity and diffusive porosity, with diffusion of mass from one to the other described by a range of rate coefficients. There is now a growing body of literature documenting the existence, observability, and effects of multiple rates of mass transfer on solute transport in the subsurface. Multiple rates of diffusive or sorptive mass transfer are theoretically and intuitively reasonable

---

Table 1. Fixed Parameters Used in Simulations

Parameter	Test				
	H11-1	H11-2	H19S2	H19S1-1	H19S1-2
Solute injection time, s	8.16×10^3	7.98×10^3	7.32×10^3	7.62×10^3	7.95×10^3
Chaser injection time, s	1.54×10^4	7.44×10^3	1.46×10^4	1.58×10^4	7.83×10^3
Pause length t_{rest}, s	6.36×10^4	6.36×10^4	6.38×10^4	6.22×10^4	6.22×10^4
Injection rate Q_{inj}, m^3/s	1.22×10^{-4}	1.27×10^{-4}	1.16×10^{-4}	1.31×10^{-4}	1.26×10^{-4}
Pumping rate Q_{out}, m^3/s	2.24×10^{-4}	2.24×10^{-4}	2.74×10^{-4}	2.37×10^{-4}	2.37×10^{-4}
Well radius r_w, m	0.065	0.065	0.113	0.113	0.113
Thickness b, m	4.4	4.4	4.4	4.4	4.4
Matrix porosity ϕ_d, dimensionless	0.160	0.160	0.147	0.147	0.147
Grid radius, m	8.00	8.00	3.75	3.75	3.75

[e.g., *Ruthven and Loughlin*, 1971; *Villermaux*, 1981; *Rao et al.*, 1982; *Cooney et al.*, 1983; *Rasmuson*, 1985; *Wu and Gschwend*, 1988; *Brusseau et al.*, 1989; *Fong and Mulkey*, 1990; *Valocchi*, 1990; *Lafolie and Hayot*, 1993; *Haggerty and Gorelick*, 1995; *Cunningham et al.*, 1997] and have been observed and modeled in a number of laboratory experiments [e.g., *Ball and Roberts*, 1991; *Connaughton et al.*, 1993; *Pedit and Miller*, 1994, 1995; *Chen and Wagenet*, 1995, 1997; *Culver et al.*, 1997; *Werth et al.*, 1997; *Haggerty and Gorelick*, 1998; *Lorden et al.*, 1998]. However, to date, there has been no field study that documents the effects of multirate diffusion.

2. Single-well injection-withdrawal tracer tests

A suite of SWIW tracer tests was conducted in the Culebra Dolomite Member of the Rustler Formation at the Waste Isolation Pilot Plant (WIPP) site in southeastern New Mexico [*Meigs and Beauheim*, this issue; *Meigs et al.*, 2000]. The Culebra is a 7-m-thick, variably fractured dolomite with massive and vuggy layers and is a potential pathway to the accessible environment in the event of a radionuclide release from the WIPP. A total of three SWIW tests were performed at two multiple-well sites, designated as the H-11 and H-19 "hydropads." SWIW tests were performed only at the central well at both hydropads. Two tests involved the injection of two tracers each, and one test involved a single tracer, resulting in a total of five SWIW data sets. The SWIW tests consisted of the consecutive injection (approximately 2 hours each) of one or more slugs of conservative tracers into the Culebra dolomite, followed by the injection of a Culebra brine chaser (containing no tracer) and then followed by a resting period of approximately 18 hours. The tracers were then removed from the formation by pumping at the same well until concentration was close to or below detection levels. The majority of tracer was removed within 48 hours of pumping, but quantifiable concentrations of tracer continued to be removed for over 1000 hours (up to 50 days) at H-11 [*Meigs and Beauheim*, this issue, Figure 7]. Mass fractions recovered over that time ranged from 0.94 to 0.98. In this paper, we will refer to the five data sets as follows: (1) the first H-19 test (SWIW1) with tracer 1 as H19S1-1; (2) the first H-19 test (SWIW1) with tracer 2 as H19S1-2; (3) the second H-19 test (SWIW2) with only one tracer added as H19S2; (4) the H-11 test (SWIW) with tracer 1 as H11-1; and (5) the H-11 test (SWIW) with tracer 2 as H11-2. A summary of key values is provided in Table 1, and details are given in Table 2 of *Meigs and Beauheim* [this issue].

3. Multirate Diffusion: Mathematical Model

In this section, we present the mathematical model used to describe advective-dispersive solute transport with multirate diffusion. The solutions to these equations are obtained in the Laplace domain and then numerically inverted using the de Hoog algorithm [*de Hoog et al.*, 1982]; the solutions are performed sequentially for each of the injection, resting, and pumping periods. Details of the solution method are presented by *Haggerty et al.* [2000a] and *Haggerty* [2000].

The multirate diffusion model is a distributed model of diffusion representing a medium with pore-scale heterogeneity in diffusive mass transfer. As conceptualized in this paper, the multirate diffusion model is similar to that described by *Cunningham et al.* [1997] and by *Haggerty and Gorelick* [1998]. Figure 1 illustrates fractures and matrix (i.e., advective and diffusive porosity) in a small volume of rock, where the matrix is heterogeneous with respect to diffusion, at spatial scales much smaller than a representative elementary volume (REV). It is assumed that this sub-REV-scale heterogeneity is replicated in approximately the same fashion everywhere in the formation.

The multirate diffusion model is a generalization of the conventional double-porosity model in that porosity is divided into two continua: advective porosity (where transport is dominated by advection and dispersion) and diffusive porosity (where transport is dominated by diffusion). However, in the multirate model the diffusion rate coefficient ($\alpha_d \equiv D_a/l^2$, see below) is described by a distribution rather than a single value. The model assumes one-dimensional diffusion along a distribution of individual pathways within matrix blocks, each with a different diffusion rate coefficient. The distribution describes the volume fraction associated with each diffusion rate coefficient. Although Figure 1 shows cubic matrix blocks in the model, the pathways and the blocks can be any shape, provided that each pathway is one-dimensional, homogeneous, and independent of other pathways. With these criteria each diffusive pathway in the distribution can be modeled with a one-dimensional diffusion equation. Also, in addition to diffusion into the rock matrix, solute may diffuse into material that fills fractures and also into pockets of immobile water adjacent to advective porosity.

Variability in the diffusion rate coefficient is due to a combination of factors, including variability in at least the following: (1) matrix block size; (2) tortuosity; (3) pore geometry; (4) restricted diffusion within pores (i.e., diffusion is slowed by
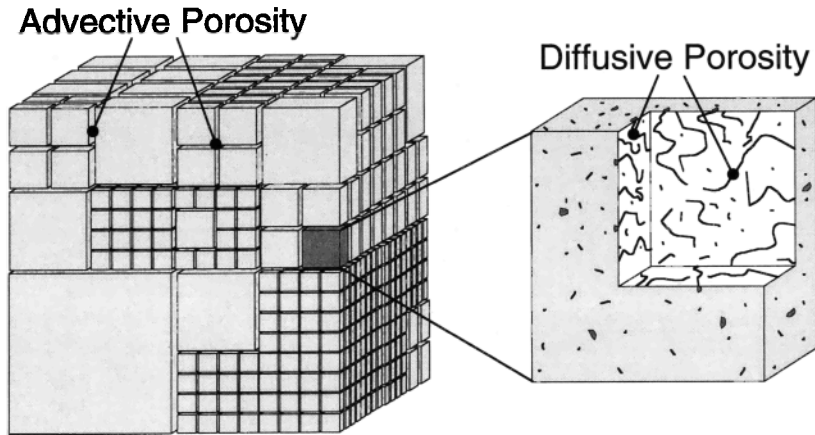
Figure 1. Conceptual model for multirate diffusion. Although the illustrated blocks are cubes, the blocks may be of any shape. The volume of rock shown in the diagram is less than the representative elementary volume.

small cross-sectional area of the pore); (5) variably sized dead-end pores adjacent to advective porosity; and (6) interaction with pore walls, including sorption (though the tracers employed in our experiments are believed to be nonsorbing). For further discussion on these sources of variability, see *Pedit and Miller* [1994], *Haggerty and Gorelick* [1995, 1998], and *Pignatello and Xing* [1996].

Variability in diffusion rate coefficients may also be a spurious consequence of heterogeneity in permeability. This will be the case whenever a mass transfer model is used to represent tailing in recovery concentrations resulting from variability in advection times. For example, *Li et al.* [1994] showed that a first-order mass transfer model was able to simulate such advective tailing but that the rate coefficient was velocity-dependent. Similar error should be expected if tailing resulted from heterogeneity but was incorrectly modeled with a distribution of diffusion rate coefficients.

The distribution of diffusion rate coefficients, D_a/l^2, may be defined in any appropriate manner but most commonly is defined as a statistical distribution. *Culver et al.* [1997], *Cunningham et al.* [1997], and others have used a gamma distribution, while *Pedit and Miller* [1994, 1995], *Haggerty and Gorelick* [1998], and others have employed a lognormal distribution. Because the diffusion rate coefficient is the product of several parameters (i.e., diffusion depth into the block, tortuosity, and constrictivity) that each have variability, a lognormal distribution is a reasonable assumption. For further discussion of the reasoning behind this choice, see *Haggerty and Gorelick* [1998].

The mathematical models presented here make the following important simplifications: (1) The regional hydraulic gradient is negligible. (2) The formation is isotropic, confined, horizontal, homogeneous with respect to groundwater flow, and of constant thickness. The second set of assumptions above simply guarantees that flow is radially symmetric. Provided that the first assumption is valid, then the issue of heterogeneity is much less significant for a SWIW test than for other types of tests, because the tracer leaves the well and comes back to the well along the same path. Therefore, although the second assumption is certainly violated within the Culebra dolomite,-the effects on a SWIW test are likely to be small [*Altman et al.*, 2000]. In the case where both the first and second assumptions are violated, the estimated diffusion parameters will contain error. This is discussed in section 5.2.

The equations for solute transport into or out of a well, in the presence of a lognormal distribution of matrix diffusion processes, are given by

$$\frac{\partial c_a}{\partial t} + \int_0^\infty b(\alpha_d) \, \frac{\partial \hat{c}_d(\alpha_d)}{\partial t} \, d\alpha_d = \frac{1}{r} \frac{\partial}{\partial r} \left(\frac{r\alpha_L |v|}{R_a} \frac{\partial c_a}{\partial r} \right) - \frac{v}{R_a} \frac{\partial c_a}{\partial r},$$

$$\text{(1)}$$

$$b(\alpha_d) = \frac{\beta_{tot}}{\sqrt{2\pi} \, \sigma_d \alpha_d} \exp \left\{ - \frac{[\ln(\alpha_d) - \mu_d]^2}{2\sigma_d^2} \right\}, \quad \text{(2a)}$$

where

$$\alpha_d \equiv D_a/l^2, \quad \text{(2b)}$$

$$\beta_{tot} = \frac{\phi_d R_d}{\phi_a R_a} \quad \text{(2c)}$$

and where $D_a \, [L^2 \, T^{-1}]$ is the apparent diffusion coefficient in the matrix, which may be defined most simply as the product of the aqueous diffusion coefficient of the tracer, the restrictivity factor, and diffusive tortuosity, although this expression may be modified to incorporate processes such as immobile zone sorption, and $l \, [L]$ is the length of the diffusion pathway within the matrix, which is nominally half the block width (though it may be less if the pore is not connected to other pores). See the notation list for definitions of all other parameters. Note that we do not consider transverse dispersion in (1) because the flow is assumed to be radially symmetric, and therefore transverse dispersion plays no role.

For later reference we note that $1/3 \, \alpha_d^{-1}$ is the mean residence time of a solute molecule in a micropore of length l or a matrix block of width $2l$, where the molecule moves only by diffusion within the micropore. We will therefore later refer to α_d^{-1} as the "diffusion timescale." Solute concentration in a fracture will be in approximate equilibrium with that in a matrix block of width $2l$ after a time of α_d^{-1}. Conversely, solute concentration in a fracture will be little changed by matrix diffusion if it remains in contact with the same matrix block for times much less than α_d^{-1}.

The time derivative of the spatially averaged solute concentration in the matrix is given by

$$\frac{\partial \hat{c}_d(\alpha_d)}{\partial t} = \frac{1}{l} \int_0^l \frac{\partial c_d(\alpha_d)}{\partial t} \, dz, \quad 0 < \alpha_d < \infty, \quad \text{(3a)}$$

where all variables are defined in the notation list. Note that l is a variable part of α_d and therefore is implicitly dependent upon α_d. The concentration at a point within the portion of the matrix associated with a particular diffusion rate coefficient is given by the solution of the diffusion equation for a one-dimensional diffusion pathway:

$$\frac{\partial c_d(\alpha_d)}{\partial t} = D_a \frac{\partial^2 c_d(\alpha_d)}{\partial z^2}, \qquad 0 < \alpha_d < \infty. \qquad (3b)$$

The boundary conditions for diffusive mass transfer are that the concentration at the edge of the matrix is equal to the concentration in the mobile zone and that the concentration gradient at the internal end of the pore or at the center of the matrix is equal to zero:

$$c_d(\alpha_d, z = l) = c_a, \qquad 0 < \alpha_d < \infty, \qquad (3c)$$

$$\frac{\partial c_d}{\partial z}(\alpha_d, z = 0) = 0, \qquad 0 < \alpha_d < \infty. \qquad (3d)$$

To solve these equations, we use the approach outlined by *Haggerty and Gorelick* [1995, 1998], where we substitute a series of first-order equations for the equations in (3a) and (3b) [see also *Haggerty*, 2000]. The substitution is done in such a way that the resulting solution for c_a is mathematically identical to that which would be obtained by solving (1)–(3d) directly. The solutions are obtained in the Laplace domain and then numerically inverted to the time domain [*Haggerty*, 2000]. The code STAMMT-R [*Haggerty et al.*, 2000a] was used to solve these equations.

To model the experiments for diffusion into a sphere [e.g., *Rao et al.*, 1980; *van Genuchten et al.*, 1985; *Ball and Roberts*, 1991], we also employ (1). However, (2a) and (3a)–(3c) are replaced by the following four equations:

$$b(\alpha_d) = \beta_{tot}\delta(\alpha_d^*), \qquad (4)$$

$$\frac{\partial \hat{c}_d(\alpha_d)}{\partial t} = \frac{3}{l^3} \int_0^l z^2 \frac{\partial c_d}{\partial t}\, dz, \qquad \alpha_d = \alpha_d^*, \qquad (5)$$

$$\frac{\partial c_d}{\partial t} = \frac{D_a}{z^2} \frac{\partial}{\partial z}\left(z^2 \frac{\partial c_d}{\partial z}\right), \qquad (6a)$$

$$c_d = c_a, \qquad z = l, \qquad (6b)$$

$$\frac{\partial c_d}{\partial z} = 0, \qquad z = 0, \qquad (6c)$$

respectively, where all variables are defined in the notation list. Equations (4)–(6c) describe diffusion in and out of a spherical matrix block, where the matrix is assumed to be homogeneous and the boundary concentrations are assumed to be the same everywhere at the surface of the sphere. Consequently, the diffusion equation (6a) is in spherical coordinates but is independent of any angle. It should be noted that the most significant feature of spherical diffusion is that there is a single value of D_a/l^2 and not that diffusion is assumed to be into a spherical matrix block.

The choice of spherical geometry for the single-rate model is not important. It has been shown by several authors that there is no significant difference between diffusion into spheres and cylinders, layers, or cubes, other than that the mean residence time differs for a fixed value of l [e.g., *Villermaux*, 1981; *Rao et al.*, 1982; *Goltz and Roberts*, 1987]. The mean residence time in a slab is 5 times the mean residence time in a sphere of the same half thickness. Therefore the multirate model for one-dimensional pathways with $\sigma_d = 0$ is approximately the same as the single-rate model provided that μ_d (multirate) = exp $(D_a/5l^2)$ (sphere).

3.1. Radially Divergent Flow (Injection Period)

For each of the three parts of a SWIW test (the injection, resting, and pumping periods), the pore water velocities, initial conditions, and boundary conditions differ. Let us first consider the injection period.

The pore water velocity in (1) during the injection period is given by

$$v = \frac{Q_{inj}}{2\pi r \phi_a b}, \qquad (7)$$

where variables are defined in the notation list and b [L] is the formation thickness. The boundary conditions for use with (1) for conditions of radially divergent flow (injection) are

$$c_a - \alpha_L \frac{\partial c_a}{\partial r} = c_{inj}, \qquad r = r_w, \qquad (8a)$$

$$\frac{\partial c_a}{\partial r} = 0, \qquad r \to \infty. \qquad (8b)$$

Equation (8a) is the flux boundary at the well accounting for dispersion, and (8b) is the boundary condition at infinity during injection. Initial conditions for radially divergent flow are that concentrations in both the advective and diffusive porosities (i.e., matrix and fracture porosities) are initially zero.

The equations described in this section must be solved over all space at the end of the injection period. We solved these equations on a one-dimensional grid (since it is assumed that concentrations change only radially away from the well). The grid used 25 equally spaced nodes and was terminated at a distance where mobile concentrations fell below 10^{-4} of injected concentration. With this number of nodes placed to the edge of the concentration field, results were insensitive to grid spacing. An independent mass balance calculation, involving an analytical solution for the mass, ensured all injected mass was accounted for.

3.2. No Flow (Resting Period)

After the injection period the well is turned off. During the resting period the pore water velocity in the formation is assumed to be zero. This is justified because velocities near a well very rapidly come to steady state after a change in pumping rate, even though heads may continue to change for some time. *Harvey et al.* [1994] discuss a method for checking this assumption. The storativity of the Culebra is 4.9×10^{-5} at H-19 and 4.5×10^{-5} at H-11. The transmissivity of the Culebra is 6.8×10^{-6} m^2 s^{-1} at H-19 and 4.7×10^{-5} m^2 s^{-1} at H-11 [*Beauheim and Ruskauff*, 1998]. Using *Harvey et al.*'s [1994] work, velocities decline to 5% of their pumping values at 2-m distance after only 2.3 min at H-19 and after only 0.31 min at H-11. Velocities decline much faster closer to the well, so these are conservative estimates of time needed to reach a resting (i.e., no movement) condition. Therefore (1) may be simplified

$$\frac{\partial c_a}{\partial t} + \int_0^\infty b(\alpha_d) \frac{\partial \hat{c}_d(\alpha_d)}{\partial t}\, d\alpha_d = 0, \qquad (9)$$

and all other equations remain the same. Since (9) is an ordinary differential equation in time, no boundary conditions are required. Initial conditions for the resting period are taken as the concentrations at the end of the injection period. Concentrations are solved at the end of the resting period, spatially along the grid discussed in section 3.1.

3.3. Radially Convergent Flow (Pumping Period)

The pore water velocity in (1) during the pumping period is given by

$$v = -\frac{Q_{out}}{2\pi r \phi_a b}. \tag{10}$$

We also assume that the velocity in (10) is constant because velocities quickly come to steady state in a radial system (see reasoning in section 3.2). The boundary conditions for use with (1) for conditions of radially convergent flow (pumping) are

$$\frac{\partial c_a}{\partial r} = 0, \qquad r = r_w, \tag{11a}$$

$$c_a = 0, \qquad r \to \infty. \tag{11b}$$

Initial conditions for radially convergent flow are that concentrations (both advective and diffusive) at every point on the grid (see the end of section 3.1) are initially identical to those at the end of the resting period. Note that (11a) is a necessary boundary condition for outflow. Strictly speaking, however, the boundary condition requires that all the flow paths have the same velocity through the well surface [Kreft and Zuber, 1986], a condition which is impossible to construct even in the laboratory. The consequences of this limitation, inherent in all models requiring this boundary condition, are that model dispersion at the well may have less dispersion at early times than the true breakthrough curve. However, since our estimations depend primarily on the late time behavior of the recovery curve, this issue should not affect our results.

4. Modeling of SWIW Tests

In this section we present two models of the SWIW tests. First, we present results from our effort to model the experiments using conventional (i.e., single rate) diffusion into a spherical matrix block and transport assuming radial flow. Second, we show the multirate diffusion model of the experimental results. We also present results from a sensitivity analysis with the multirate diffusion model, including confidence bounds on the parameter estimates.

Parameters used by the models were defined in one of two ways: (1) Values were fixed based on knowledge of the tracer tests and the Culebra geology. (2) Values were estimated by fitting the models to the data [Meigs and Beauheim, this issue]. All parameters that could be fixed are shown in Table 1. Although all tests except H19S2 were injected over the full thickness of the Culebra (Table 2), we used a model thickness of 4.4 m, representative of the lower Culebra. Since the lower Culebra has much higher permeability than the upper Culebra [Meigs and Beauheim, this issue], this is appropriate. In any case, dimensional analysis indicates that thickness and advective porosity are strongly correlated. As such, an error in the assumed thickness will lead to a different estimate of advective porosity.
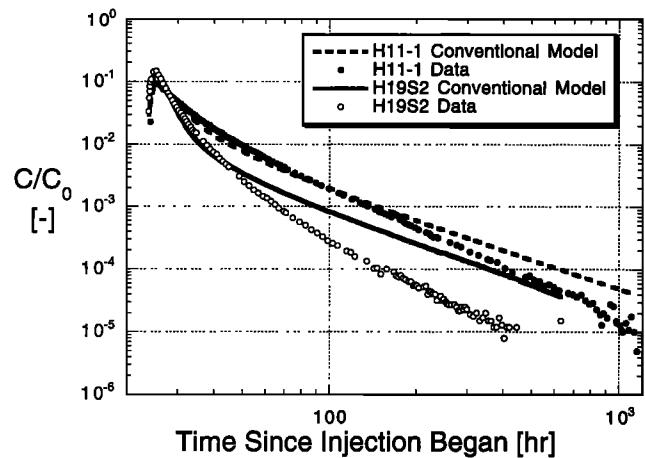
Estimation of parameters was done using a nonlinear least

Figure 2. Best fits of conventional double-porosity models to the H11-1 and H19S2 data. Parameters are given in Table 2.

squares algorithm [e.g., Marquardt, 1963]. For each data set and model of that data we found the set of parameters that minimized the sum of squared errors on the logarithm of concentrations. Logs of concentrations were used because we are trying to understand diffusive mass transfer, which most strongly influences small concentrations at late time (this influence can be seen in plots of the Jacobian, Figure 5, discussed in section 5.1). We estimated the natural logs of those parameters that are strictly positive-valued. For purposes of comparison we used the root-mean-square error (RMSE), defined for natural logs of concentration and corrected for the number of parameters estimated [e.g., Bard, 1974, p. 178]. A first-order approximation to the estimated parameter covariance matrix (V_p) is given by [e.g., Bard, 1974; Draper and Smith, 1981]

$$V_p = \sigma^2 (J^T J)^{-1}, \tag{12}$$

where σ is the replicate variance defining the uncertainty in concentration (assumed to be uniform and equal to the RMSE) and J is the Jacobian, which is the matrix of sensitivities of the model output to the parameter estimates. In the analyses that follow, σ_p is the standard deviation of the estimated parameter, which is the square root of the respective diagonal from V_p.

4.1. Conventional Double-Porosity and Radial Transport

Figure 2 shows the best obtainable fit of the conventional double-porosity model to the H19S2 and H11-1 recovery curves. Recall that the conventional double-porosity model includes advection (in this case, in radial coordinates), longitudinal dispersion, and diffusion into a single size class of spherical blocks. Modeling of the other recovery curves is not shown for conventional double porosity because the two attempts with H19S2 and H11-1 clearly demonstrate that a conventional double-porosity model is inadequate. The parameters estimated from these fits and the RMSEs are given in Table 2.

We used only early time data (first 50 hours) in the inversion procedure, roughly corresponding to the advection/dispersion-dominated part of the recovery curve. This was necessary because it was found that the conventional double-porosity model could not possibly match the late time data (see Figure 2). When matching the late time data was attempted, other estimated parameters in the model were made physically un-

Table 2. Single-Rate Double-Porosity Estimation Results[a]

Test	Log [Mean (α_d)] μ_d	Advective Porosity ϕ_a, dimensionless	Dispersivity α_L, m	RMSE
H19S2	−16.2	0.0540	0.159	1.27
H11-1	−18.8	0.00714	0.458	0.527

[a]Note that $\alpha_d \equiv D_a/l^2$.

reasonable (e.g., advective porosity close to 100% or dispersivity larger than several meters, close to the spatial scale of the experiment), and the estimation algorithm would fail. In dozens of scoping runs with a conventional double-porosity model, no set of parameters was able to reproduce the late time slope of the data. For conventional double-porosity models the slope is −1.5 for times after the advectively dominated early part of the test and before the diffusion timescale of approximately l^2/D_a [*Tsang*, 1995; *Hadermann and Heer*, 1996]. At times greater than the diffusion timescale, the double-log slope predicted for a conventional double-porosity model quickly goes to infinity (in other words, the matrix is quickly emptied of solute once the diffusion timescale is reached). Also note that the geometry of the matrix block, assumed to be spherical, is not important. As discussed in section 3, the geometry only influences the mean residence time in the matrix and not the shape of the tail of the recovery curve. For these reasons we also decided not to produce confidence bounds on the parameter estimates shown in Table 2.

4.2. Multirate Diffusion and Radial Transport

Figures 3a–3e show the multirate diffusion model results (assuming a lognormal distribution of rate coefficients) of the five SWIW recovery curves. Recall that the multirate diffusion model includes advection (in this case, in radial coordinates), longitudinal dispersion, and diffusion into matrix with a distribution of diffusion rate coefficients.

From Figures 3a–3e we note two points. First, the data from all five SWIW data sets are fit very well by the multirate diffusion model. The RMSE values (Table 3) range from 0.150 to 0.424, which are 4–8 times smaller than the conventional double-porosity model for the same respective SWIW data sets. This improvement over the conventional double-porosity model is achieved with one additional estimated parameter. Second, the models fit the observed recovery curves over the entire range of data, including both early and late concentrations.

The parameters estimated from these fits, their 95% confidence intervals (i.e., $2\sigma_p$), and the associated RMSEs are given in Table 3. Since the natural logarithms of positive-valued parameters were estimated, the confidence intervals are on the logs of the estimates for all parameters except μ_d. From Table 3 we note four points. First, the parameters indicate that the estimated distribution of μ_d (diffusion rate coefficient) is very broad, spanning several orders of magnitude. Second, the distribution of α_d appears to be different at H-11 than at H-19. This is discussed below in more detail. Third, μ_d and σ_d have relatively small confidence intervals, while ϕ_a and α_L generally have very large confidence intervals. In particular, we note that the confidence interval on the estimate of advective porosity suggests that this parameter is essentially unestimable in a SWIW test. Conversely, σ_d appears to be particularly well measured by this type of test. However, the terms "large" and "small" are somewhat subjective, and a more detailed analysis

is given in section 5. Fourth, parameters estimated from tests at the same well (with the exception of σ_d for the H19S1-2 recovery curve) have values that are statistically the same (i.e., their confidence intervals greatly overlap).

Figure 4 shows the estimated cumulative distribution functions (CDFs) of the diffusion rate coefficient for the five models. The graph shows the cumulative matrix volume associated with a diffusion rate coefficient smaller than a given value. The variance of the estimated distribution is large for all tests but is somewhat larger, in general, for the H-19 tests than for the H-11 test. The estimated CDFs display 95% of the distribution spanning a range of 4.4–11.7 orders of magnitude. We also note that the CDFs from the H-11 and H-19 tests appear to be self-consistent, with the exception of CDF for H19S1-2, which has a different estimated σ_d than the other two at H-19 (discussed in section 5.3).

Figure 4 contains a shaded region, indicating the portion of the CDF of diffusion rate coefficients that could be assayed (i.e., "observed") by the tracer tests. Upper and lower limits were calculated by considering the diffusion timescale (see discussion following (2c) for definition) for different parts of the CDF. For example, a matrix block or one-dimensional micropore that is characterized by α_d of 2.3×10^{-9} s^{-1} would require approximately 4.3×10^8 s (1.20×10^5 hours) for solute to diffuse into it. Therefore we recognize that such a micropore could not measurably affect a tracer test at timescales 100 times smaller (of the order of 1200 hours, the time of the last data point in H11-1). This reasoning is consistent with arguments based on Damkohler numbers (proportional to the advection timescale divided by the diffusion timescale) [e.g., *Bahr and Rubin*, 1987]. Therefore we draw an approximate lower limit of the shaded zone at 2.3×10^{-9} s^{-1}. Thus the portion of the CDF with values of α_d smaller than the shaded region corresponds to that part of the diffusive porosity that could not be assayed by the SWIW tests. A longer-duration test would be needed to "observe" that portion of the matrix. Note that this diffusion rate coefficient corresponds to a diffusion pathway length l of 0.187 m (calculated for a tortuosity of 0.11 and a diffusivity of 7.3×10^{-10} m^2 s^{-1}, which is appropriate for 2,4-DCBA, used in H11-1, H19S1-1, and H19S2).

On the other end of the timescale spectrum, diffusive mass transfer that is very fast will be obscured by advective processes. Since we do not know the ratio of advective to diffusive porosity, it is impossible to distinguish between pores dominated by advection and small micropores into which diffusion occurs quickly. In other words, the influence of rapid diffusion on the recovery curve is indistinguishable from the effect of advective porosity on the recovery curve. Therefore the fastest observable diffusion processes will occur at a minimum of approximately 1% of transport time through the system. For our system this initial recovery time also includes the injection and resting time (a total of about 24 hours), which corresponds to α_d of 1.2×10^{-3} s^{-1}. The fastest observable diffusion
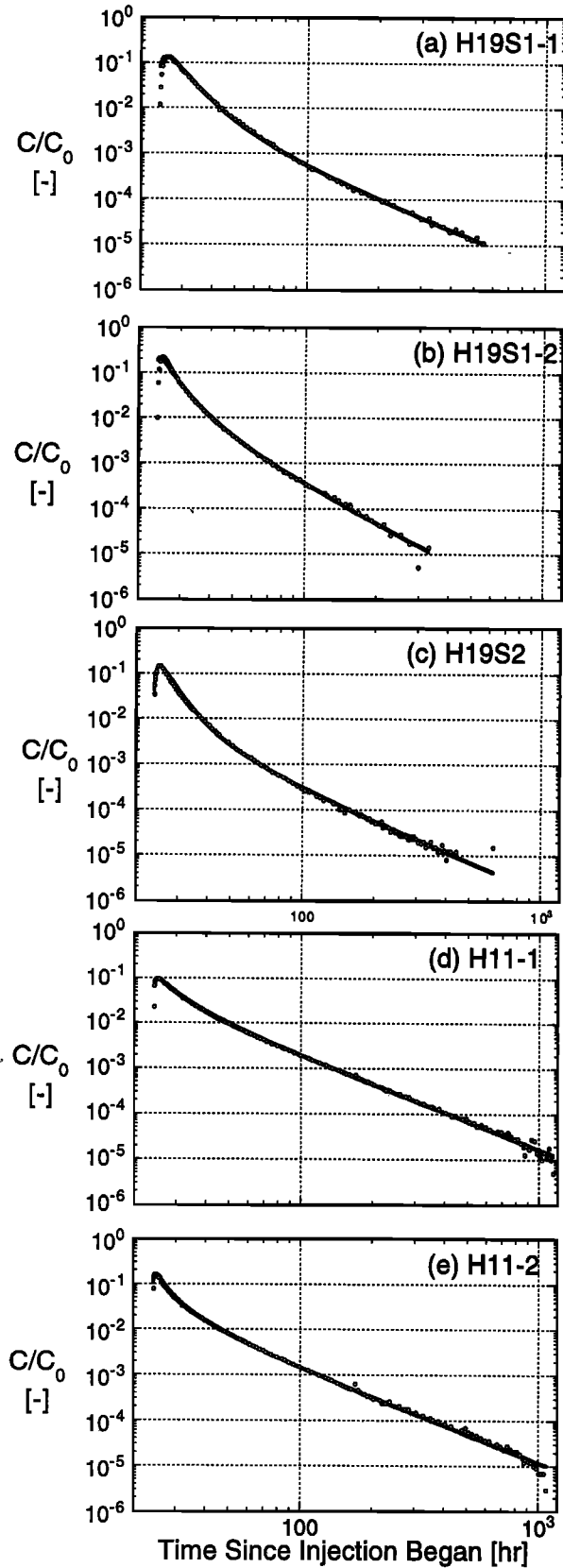
Figure 3. Best fits of multirate diffusion model to all single-well injection-withdrawal (SWIW) data for tests: (a) H19S1-1, (b) H19S1-2, (c) H19S2, (d) H11-1, and (e) H11-2. Parameters are given in Table 3.

Table 3. Multirate Estimation Results[a]

| Test | Log [Mean (α_d)][b] | | Standard Deviation Log (σ_d)[c] | | | Advective Porosity | | | Dispersivity | | | RMSE |
	$\mu_d \pm 2\sigma$[c]	Range	σ_d	$\ln(\sigma_d) \pm 2\sigma$	Range	ϕ_a, dimensionless	$\ln(\phi_a) \pm 2\sigma$	Range	α_L, m	$\ln(\alpha_L) \pm 2\sigma$	Range	
H11-1	-15.8 ± 1.09	$-14.7, -16.9$	3.55	1.27 ± 0.245	2.79, 4.54	0.00175	-6.35 ± 4.59	$1.77 \times 10^{-5}, 0.174$	0.0566	-2.87 ± 4.35	$7.33 \times 10^{-4}, 4.37$	0.150
H11-2	-15.7 ± 0.942	$-14.7, -16.6$	3.83	1.34 ± 0.238	3.02, 4.858	0.00430	-5.45 ± 2.53	$3.43 \times 10^{-4}, 0.0538$	0.0365	-3.31 ± 5.08	$2.28 \times 10^{-4}, 5.84$	0.152
H19S2	-10.9 ± 1.67	$-9.23, -12.5$	5.83	1.76 ± 0.237	4.60, 7.38	0.0151	-4.19 ± 2.74	$9.78 \times 10^{-4}, 0.233$	0.173	-1.76 ± 0.237	0.136, 0.219	0.161
H19S1-1	-11.9 ± 3.96	$-7.94, -15.9$	6.87	1.93 ± 0.297	5.12, 9.272	0.00485	-5.33 ± 12.8	$1.34 \times 10^{-8}, >1$	0.213	-1.55 ± 0.356	0.149, 0.303	0.276
H19S1-2	-10.1 ± 3.98	$-6.12, -14.1$	2.56	0.940 ± 0.822	1.13, 5.83	0.0202	-3.90 ± 12.7	$6.18 \times 10^{-8}, >1$	0.117	-2.15 ± 1.80	0.019, 0.705	0.424

[a]For a given test the first entry under each straddle rule (except that for μ_d) gives the best fit parameter value; the second entry row gives the natural logarithm of the best fit parameter value and 95% confidence limits; and the third row gives the range of possible parameter values to within 95% confidence.

[b]Note that $\alpha_d = D_a/l^2$. See text for details.

[c]Here μ_d was directly estimated (as opposed to its logarithm), so confidence limits are given in arithmetic space.
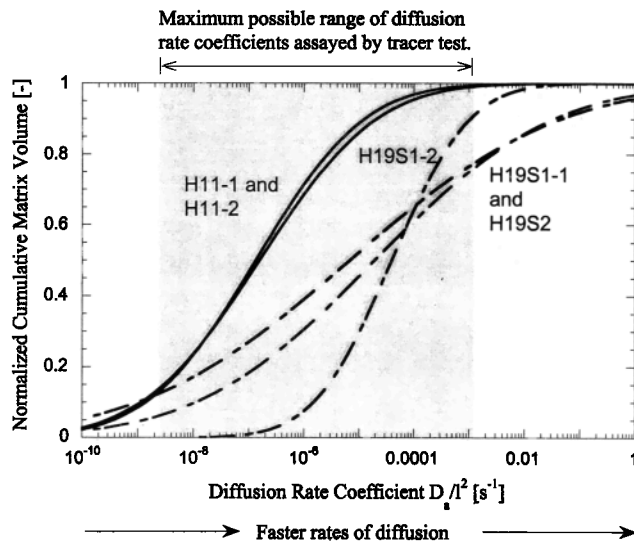
Figure 4. Cumulative distribution functions (CDFs) estimated from each of the SWIW data. CDFs shown here correspond to the models shown in Figure 3 and the parameters given in Table 3.

process is probably slower than this, but this provides an approximate upper bound. Note that this diffusion rate coefficient corresponds to a diffusion pathway length l of 0.259 mm (calculated for a tortuosity of 0.11 and a diffusivity of 7.3 $\times$ 10^{-10} m^2 s^{-1}).

The fringes of the estimated CDFs, lying outside the bounds in Figure 4, are highly nonunique and are not supported by data. They appear on the CDF only because we have chosen, a priori, a lognormal distribution. We have the largest degree of confidence about the part of the CDF near the center of the shaded region, with decreasing confidence toward the edges. For a detailed discussion of the confidence intervals on a distribution of rate coefficients, see *Hollenbeck et al.* [1999].

As discussed above, the estimated CDFs suggest that 95% of the distribution is spread over 4.4–11.7 orders of magnitude. However, not all of this distribution is supported by data. If the unsupported portions of the CDFs are ignored, the distributions are spread over 3.6–5.7 orders of magnitude. This spread should be considered a minimum, as a longer-duration experiment would likely support a wider spread.

5. Discussion

5.1. Model Sensitivity to Estimated Parameters

In this section we discuss the sensitivity of the multirate diffusion model to the estimated parameters. The Jacobian (sensitivity matrix of dependent variable to model parameter) can be normalized to allow comparison of parameter sensitivities through time and from one parameter to another [*Harvey et al.*, 1996]:

$$J_{ij} = \frac{p_j}{\sigma} \frac{\partial C_i}{\partial p_j}, \qquad (13)$$

where variables are defined in the notation list. The Jacobian is a useful instrument for investigating the sensitivity of the model to the estimated parameters as a function of time [e.g., *Wagner and Harvey*, 1997] and gives insight into the correlation between estimated parameters. A large value (either positive

or negative) in the Jacobian indicates that the model, at a particular time, is sensitive to a given parameter; a small value would indicate that the model is insensitive to the parameter. The parameter covariance matrix from (12) was also used to examine cross correlation.

Plots of the columns of the Jacobians for H11-1 and H19S2 are given in Figures 5a and 5b, respectively; each is representative of the sensitivity matrices computed for other SWIW tests at their respective locations. In both plots it is clear that the nature of all sensitivities changes significantly between the advection/dispersion- and mass transfer-dominated parts of the simulations, a transition which occurs at roughly 40 hours (1.44 $\times$ 10^5 s) at the H-11 well and at roughly 30 hours (1.08 $\times$ 10^5 s) at H-19.

For H11-1 the sensitivity of the model to the mass transfer parameters is much larger than to the flow parameters and increases over time. The sensitivities to dispersivity and advective porosity are small and essentially constant for times greater than 40 hours, suggesting strong correlation. Consequently, neither parameter can be estimated with any confidence. In contrast, the sensitivities of the mean and standard deviation of the distribution of log diffusion rate coefficients are larger and increase through time. Thus the mass transfer parameters can be estimated with a reasonable degree of confidence, provided that good data are available at late time. These conclusions are supported both by the covariances and by the confidence intervals of the estimated parameters (see Table 3).

The sensitivity matrix for H19S2 exhibits greater complexity than H11-1. First, μ_d shows a fairly high degree of correlation with ϕ_a, but the sensitivities are somewhat larger for ϕ_a than
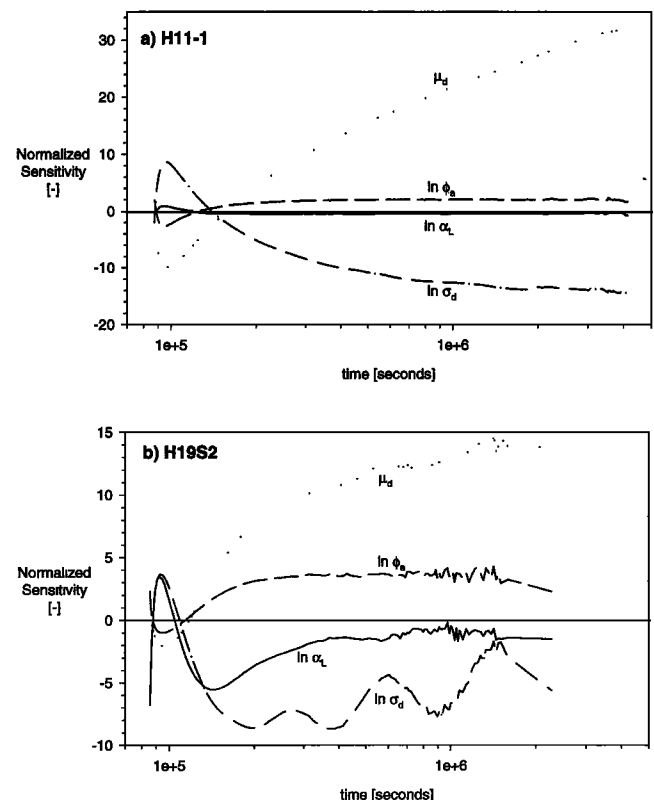

Figure 5. Normalized sensitivity for estimated parameters of multirate diffusion model at (a) H11-1 and (b) H19S2.

in H11-1. This is explained as follows. The largest values in the distribution of diffusion rate coefficients represent near-instantaneous mass transfer. Hence the corresponding diffusive porosity effectively acts as part of the advective porosity (i.e., they are indistinguishable). The fraction of the distribution of diffusion rate coefficients that are large is determined in part by μ_d (larger μ_d means that the geometric mean of α_d is larger and diffusive mass transfer is faster). Therefore μ_d determines the fraction of the diffusive porosity that is indistinguishable from advective porosity. Consequently, μ_d and ϕ_a can be strongly correlated if μ_d is relatively large (as is the case in H19S2). Nonetheless, μ_d can still be estimated with reasonable confidence, though with less confidence than in H11-1.

Second, in H19S2 the sensitivities exhibit a higher degree of scatter and numerical error. The scatter and oscillations in the sensitivity plot are due to numerical error at very low concentrations and do not have physical significance. Sensitivities are calculated numerically as derivatives, which are very sensitive to small numerical errors.

5.2. Model Sensitivity to Heterogeneity and Tracer Drift

We have shown in sections 4.2 and 5.1 that, in the absence of either heterogeneity or drift, the late time behavior of the SWIW test is very sensitive to matrix diffusion. In this section we turn our attention to the sensitivity of the multirate diffusion model to heterogeneity in permeability and tracer drift due to a regional hydraulic gradient.

Without heterogeneity, drift does not significantly affect the late-time behavior of the SWIW. Similarly, without drift, heterogeneity does not significantly affect the late time behavior of the SWIW [*Lessoff and Konikow*, 1997; *Altman et al.*, 2000]. However, under some conditions the combination of drift and heterogeneity can influence the late-time concentrations and therefore bias the estimate of diffusion parameters. In particular, *Lessoff and Konikow* [1997] showed that when a tracer moves away from the well in a channel of high permeability, then drifts into a lower permeability zone, and then is pulled back to the well through that low permeability zone, significant tailing in the recovery curve can result. This tailing may result in incorrect estimates of diffusion parameters.

To investigate the effects of combined heterogeneity and drift on our estimated parameters, *Altman et al.* [2000] used a particle tracking algorithm to simulate 100 SWIW tests in different heterogeneous transmissivity fields, with parameters similar to those used at the H-11 hydropad. The transmissivity (T) fields were generated using sequential Gaussian simulation; they had a mean T of 5.1×10^{-5} m^2 s^{-1}, a ln (T) variance of 3.10, and a correlation length of 15.0 m. The largest reasonable regional hydraulic gradient (0.011) was used. We selected the calculated recovery curve with the most gradual mass recovery rate (i.e., the simulation with a tail that looked most like diffusion). We then simulated the same SWIW test using an advection-dispersion model (SWIFT II [*Reeves et al.*, 1986], which is capable of simulating diffusion for a SWIW test, whereas the particle tracking code is not) with a longitudinal dispersivity of 0.25 m and a transverse dispersivity of 0.025 m. This breakthrough curve is shown in Figure 6 as a dotted line with the legend caption "Model with drift and heterogeneity."

To investigate the influence of heterogeneity on the multirate model, we performed parameter estimation on this breakthrough curve assuming that a lognormal distribution of diffusion rate coefficients was responsible for the late time behavior. The resulting curve fit is shown in Figure 6 as a solid
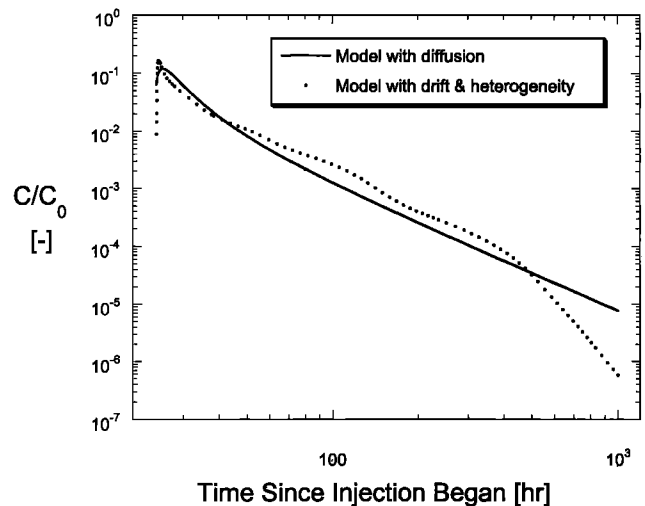

Figure 6. Best fit of multirate diffusion model to SWIW model incorporating both heterogeneity and drift.

line with the legend caption "Model with diffusion." The resulting multirate fit yielded $\mu_d = -14.1$, $\sigma_d = 3.96$, $\alpha_L = 9.05 \times 10^{-2}$ m, $\phi_a = 6.21 \times 10^{-3}$, and RMSE = 0.879.

Although the multirate model erroneously attributes the late time behavior from the heterogeneous field to diffusion, the resulting model is a very poor representation of the breakthrough curve. As such, it would be inappropriate to attribute such breakthrough curve behavior to multirate diffusion. First, the RMSE is much larger than any of the values obtained from fits to real data (see Table 3). The increased error is primarily due to the "bumpy" nature of the late time simulated concentrations from the heterogeneous field. Second, the heterogeneous field results in a breakthrough curve at very late time (i.e., after 500 hours) that is much steeper than the multirate breakthrough curve. Whereas conventional advective-dispersive behavior results in exponential late time behavior (i.e., steepening breakthrough curves on a log-log plot), multirate diffusion typically results in approximately power law behavior at late time (i.e., straight breakthrough curves on a log-log plot). Third, it must be remembered that this transmissivity field was chosen by hand from 100 random cases as the one that most closely yielded diffusion-like behavior at late time.

While it would be inappropriate to attribute late time behavior in Figure 6 to diffusion, the investigation shows that the late time behavior can be influenced by a combination of heterogeneity and drift. In particular, the combination of heterogeneity and drift may result in overestimation of the variability in the diffusion rate coefficient.

5.3. Discussion of Estimated Parameters and Comparison With Other Data

In this section we will discuss the estimated parameters and their confidence intervals and compare these values to data external to the SWIW tests. The values of ϕ_a and α_L (see Table 3) cannot confidently be estimated by the SWIW test: Both parameters have extremely large confidence intervals. In the case of ϕ_a the confidence intervals span all possible values of advective porosity. Dispersivity has slightly smaller confidence intervals, but the confidence intervals still span all possible values. Surprisingly, however, all estimated values of both

ϕ_a and α_L are in reasonable agreement with independent information. The estimated values of α_L, for example, lie within the bounds of field-scale dispersivities observed in other types of tests at similar scales [Gelhar et al., 1992]. The advective porosities we estimate are within the range expected for fractured rock and lie at the upper end of the range observed from multiwell tests in the Culebra [McKenna et al., this issue].

Advective porosity and dispersivity are not estimable by a SWIW test because the flow field is reversed in the middle of the experiment. Large and small values of these two parameters result in very similar early time breakthroughs, and the late time breakthrough is almost completely insensitive to the parameters. In contrast, diffusion is not affected by the reversal of the flow field. Additionally, the late time breakthrough is very sensitive to diffusive mass transfer. Consequently, the parameters describing the distribution of diffusion rate coefficients, μ_d and σ_d (discussed below), are quite estimable in a SWIW test.

The parameters μ_d and σ_d are estimated with smaller confidence intervals relative to their range of reasonable values. Because diffusion rate coefficients can vary over an extremely wide range, 95% confidence intervals on μ_d of about ±1–2 indicate a reasonable degree of confidence for this parameter. The value of $\ln(\sigma_d)$ appears to be well estimated by the SWIW test also (with the exception of H19S1-2, which is a much shorter data set). Other than H19S1-2, the confidence intervals on $\ln(\sigma_d)$ range from ±0.24 to ±0.30.

The mean and standard deviation of diffusion rate coefficients were both generally larger for H-19 recovery curves than for H-11 recovery curves. This corresponds well to our current understanding of the hydrogeology at the two hydropads. On the basis of advective porosities inferred from multiwell convergent-flow tracer tests [McKenna et al., this issue], transmissivities determined for many wells at the WIPP site [Beauheim and Ruskauff, 1998; Holt, 1997], and examination of drill core [Holt, 1997], it is believed that advective transport in the Culebra dolomite at the H-11 hydropad tends to be channeled along well-connected fractures that form comparatively direct flow paths. At the H-19 hydropad, advective porosity consists not only of fracture porosity but also interparticle porosity and vugs connected by microfractures, and flow thus follows a more circuitous route [Meigs et al., 2000]. Mass that is advectively transported near the H-11 hydropad experiences: (1) exposure to a smaller surface area of matrix, resulting in less matrix diffusion during a given timescale or space scale of experiment and thus slower diffusion rates, and (2) incomplete exposure to the range of porosity types, resulting in a narrower spread to the distribution of diffusion rate coefficients.

The distributions of α_d estimated from the SWIW tests appear consistent from test to test and data set to data set, with the exception of H19S1-2. The H-11 data set and the other two H-19 data sets yielded very similar values of μ_d and σ_d for tests conducted at the same well. The estimated values of μ_d and σ_d for H19S1-2 are larger and smaller, respectively, than for H19S2 and H19S1-1. The confidence interval on σ_d for H19S1-2 is large enough, however, that the value of σ_d is very uncertain.

The larger uncertainty and different estimates of μ_d and σ_d at H19S1-2 may be due to two factors. First, the H19S1-2 data set is the shortest, with several hundred hours less data than the other H-19 data sets. The tracer sampled a smaller range of mass transfer timescales and is therefore insensitive to the slowest rates of mass transfer. This resulted in a larger esti-

mated mean diffusion rate coefficient and a lower estimated standard deviation. The influence of the timescale of the experiment on the estimated parameters was confirmed by performing a parameter estimation on a H19S1-1 data set truncated to the length of the H19S1-2 data. The resulting estimates for μ_d and σ_d from this scoping run were intermediate between those from the H19S1-1 and H19S1-2 runs.

Second, the Culebra is heterogeneous. Of the three SWIWs at H-19 the H19S1-2 injection was conducted over the smallest volume of the Culebra [Meigs and Beauheim, this issue]. As a result, H19S1-2 experienced the smallest amount of heterogeneity and therefore may be expected to have a smaller estimated σ_d.

The CDFs of diffusion rate coefficients ($\alpha_d \equiv D_a/l^2$) estimated from all recovery curves have a large standard deviation (2.56–6.87). As discussed in section 1, variability in the diffusion rate coefficient stems from multiple sources. For a nonsorbing solute these may be mathematically grouped into variability in the apparent diffusivity D_a and the length of the diffusion pathway may be squared l^2 [also see Haggerty and Gorelick, 1998], where the variability in the apparent diffusivity is itself a function of tortuosity and restrictivity. Work by Tidwell et al. [2000] and by Fleming [1998] suggests that the log of D_a in the Culebra may have a standard deviation up to approximately 1.0. If $\ln(D_a)$ has a standard deviation of 1.0, then a standard deviation in $\ln(D_a/l^2)$ of 5 (for example) would be explained by a minimum standard deviation in $\ln(l)$ of 2. This would require that 95% of the diffusion path lengths are spread over about 3.5 orders of magnitude in size. Though this is probably approaching a maximum feasible limit on variability in l, it is not unreasonable. It also must be remembered that some of the width of the estimated distribution is likely due to diffusion into immobile pockets of water and to two potential sources of error: (1) assumption of a lognormal distribution and (2) effects of combined heterogeneity and drift attributed to diffusion.

The portions of the CDFs that are supported by recovery data span at least 3.6 orders of magnitude (i.e., accounting for problems with the assumption of the lognormal distribution, see section 4.2 and above). The significance of this for long-term solute transport in the Culebra is as follows. Diffusive mass transfer results in the apparent solute transport velocity (i.e., defined as the time derivative of the first spatial moment) decreasing as a function of time [e.g., Quinodoz and Valocchi, 1993]. A distribution of diffusion rate coefficients means that the decrease in velocity occurs over a longer period of time than if there were a single diffusion rate coefficient. A spread in the diffusion rate coefficients of at least 3.6 orders of magnitude means that the tracer velocity will decrease over at least 4–6 orders of magnitude in time.

5.4. Late-Time Slope of the Data

The SWIW data shown in Figure 3 have late time slopes that are nearly constant after 200 hours (i.e., the recovery curves exhibit power law behavior). Plots of the derivatives of these log-transformed data reveal that both H-11 data sets have a constant late time slope of approximately −2.1. The late time slopes for H19S1-1 and H19S2 are both approximately −2.2, while the late time slope for H19S1-2 is approximately −2.8. For all five SWIW data sets these slopes are remarkably different from those predicted for a conventional double-porosity model. For a conventional double-porosity model the slope is −1.5 for times after the advectively dominated early part of the
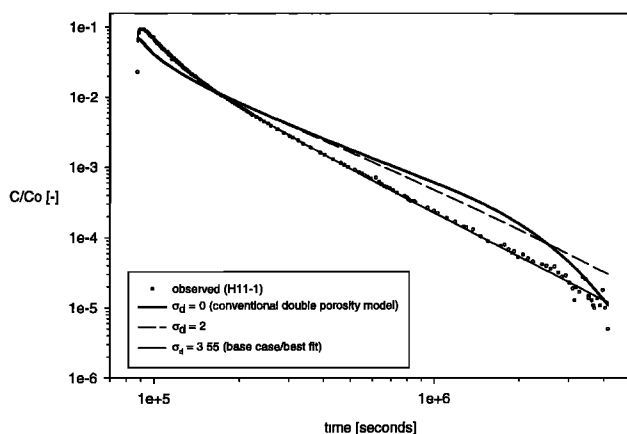
Figure 7. Sensitivity analysis for σ_d (standard deviation of ln (α_d)) in multirate diffusion model. The curve for $\sigma_d = 0$ is equivalent to the conventional double-porosity model. Prior to 2×10^5 s, the curves for $\sigma_d = 0$ and $\sigma_d = 2$ are approximately the same.

test and before the diffusion timescale of approximately l^2/D_a [*Hadermann and Heer*, 1996]. At times greater than the diffusion timescale, the slope predicted for a conventional double-porosity model quickly goes to infinity.

Figure 7 shows the effect of varying σ_d from 0 (conventional double porosity) to the estimated value of 3.57 for H11-1. For the conventional double-porosity model we see that the slope of the graph is -1.5 from ~100 to 500 hours (3.6×10^5 s to 1.8×10^6 s). However, after 500 hours the slope steepens considerably and would ultimately go to $-\infty$ as all mass is removed from the single-rate immobile zone. For the multirate diffusion models the late-time slopes are nearly constant, with values of -1.9 for $\sigma_d = 2.00$ and -2.1 for $\sigma_d = 3.5$.

In all of the SWIW data sets the late time slope is both constant and steeper than -1.5. We ran the multirate model for a range of parameters (many are not shown) and found that the late time slopes are always approximately constant and steeper than -1.5 for σ_d greater than 0. In addition, data from other types of tests (e.g., multiwell convergent-flow tests and one-dimensional column experiments with a pulse or square-wave injection) also show straight line recovery curves at late times with slopes greater than -1.5, and scoping runs performed on these data have required nonzero values for σ_d in order to adequately match the entire length of the recovery curve. Therefore we suggest that a nearly constant late time slope steeper than -1.5 for a pulse injection (either Dirac or short square wave) tracer test is diagnostic of multirate mass transfer, provided that the late time behavior is due to mass transfer. These late time behaviors are examined in detail by *Haggerty et al.* [2000b]. It is important to note, however, that other effects (not believed to have influenced the SWIW tests we examined [see *Meigs et al.*, 2000] may produce slopes similar to multirate diffusion; these include significant tracer drift, the injection well or port not being cleared of solute, or nonlinear sorption.

5.5. Conventional Double-Porosity Versus Multirate Diffusion

A growing body of literature has concluded that multirate diffusion is a significant phenomenon. The majority of this literature has shown that the estimated distributions of rate

coefficients have surprisingly large variances, even in relatively homogeneous media. It is not straightforward to compare the various models directly because of different mathematical formulations, but *Pedit and Miller* [1995], *Culver et al.* [1997], *Werth et al.*, [1997], *Haggerty and Gorelick* [1998], and *Lorden et al.* [1998] all found variability in mass transfer rate coefficients that span many orders of magnitude. Our study, based on field experiments, adds to this list. Estimated variability in the diffusion rate coefficient spans at least 5 orders of magnitude (see Figure 4). In our study we find that it is not possible to fit all parts of the field data using a conventional, single-rate double-porosity model (assuming diffusion into spherical blocks). It is possible to fit the earliest data, but these data are dominated by advection rather than mass transfer.

6. Conclusions

1. A double-porosity model incorporating distributed diffusion, such as the multirate diffusion model presented here, may be necessary to represent the recovery curves in the SWIW tests in the Culebra dolomite. A conventional, single-rate double-porosity model, assuming spherical diffusion, is not able to reproduce the observed late time slope of the data. This is a serious shortfall of the conventional double-porosity model, because the late time data are dominated by diffusive mass transfer. The portion of the recovery curve matched well by the conventional double-porosity model is dominated by advection and dispersion.

2. Parameter estimation and sensitivity analyses indicate that the SWIW tests in the Culebra dolomite are generally insensitive to advective porosity and dispersivity. This is due to the reversing flow field, in which the tracer goes out from the well and returns to the well along approximately the same flow path. However, the SWIW tests appear to be particularly sensitive to matrix diffusion, and from these tests it is possible to estimate a distribution of diffusion rate coefficients with a reasonable degree of reliability, although care must be taken to address the effects of data length and quality and the nonuniqueness of the estimated lognormal distribution of diffusion rates outside the assay range of a given tracer test.

3. The late time data are particularly sensitive to the distribution of diffusion rate coefficients. In fact, the sensitivity to the distribution generally grows through time. Therefore accurate estimation of the distribution relies on accurate concentration data in the tail of the test, where the effects of matrix diffusion dominate the effects of advection and dispersion. It is unlikely that distributions of rate coefficients can be estimated from SWIW recovery curves that either do not contain the tail concentrations or have very low accuracy tails.

4. The late time slope of the recovery curves obtained from SWIW tests in the Culebra dolomite have constant double-log slopes between approximately -2.1 and -2.8. Late time slopes obtained from conventional double-porosity models, however, are -1.5 before the diffusion timescale l^2/D_a [*Hadermann and Heer*, 1996] and quickly go from -1.5 to a slope approaching infinity after the diffusion timescale. Therefore, provided that diffusion is the explanation for the late time behavior, a constant late time slope steeper than -1.5 is diagnostic of a distribution of diffusion rate coefficients. More detail on such power law behavior is presented by *Haggerty et al.* [2000b].

5. The estimated distribution of diffusion rate coefficients is very broad for the Culebra dolomite (note caution below, however). The estimated CDFs, which assume a lognormal

distribution of rate coefficients, have a standard deviation in ln (α_d) from 2.56 to 6.87. The portions of these CDFs that are supported by data are spread over at least 3.6 orders of magnitude. Consequently, if these distributions were accurate for the entire formation, it would take approximately this many orders of magnitude in time to experience all of the mass transfer variability in the formation. Therefore the advection velocity of a solute in the Culebra would continue to slow over at least 3.7–5.7 orders of magnitude in time and possibly much longer. Any experiments or modeling conducted within these time frames would need to account for a distribution of mass transfer rate coefficients in order to accurately predict advective velocities on another timescale. Implications of such multirate diffusion for transport at larger scales is discussed by McKenna et al. [this issue].

6. Solute drift and heterogeneity in permeability are individually insufficient to create the late time behavior observed in the SWIW recovery curves. However, when both heterogeneity and drift are present, late time behavior similar to multirate mass transfer can occur. Although it is clear that multirate diffusion occurs in the Culebra, the number of orders of magnitude of variability may be overestimated because of the combined effects of drift and heterogeneity.

Notation

b formation thickness [L].

$b(\alpha_d)$ probability density function of diffusion rate coefficients (see (2a)) [T].

c_a solute concentration in the advective porosity [$M L^{-3}$].

c_d solute concentration at a point within the portion of the matrix associated with a particular diffusion rate coefficient [$M L^{-3}$].

$\hat{c}_d(\alpha_d)$ average solute concentration in the portion of the matrix associated with a particular diffusion rate coefficient [$M L^{-3}$].

C_i ith component of the vector of normalized concentrations through time [dimensionless].

c_{inj} is the injected concentration (which may be a function of time) [$M L^{-3}$].

D_a apparent diffusivity in the matrix [$L^2 T^{-1}$].

J Jacobian sensitivity matrix.

J_{ij} sensitivity of the modeled concentration at the ith time to the jth parameter.

l length of the diffusion pathway within the matrix. Note that this becomes the radius if the matrix block is a sphere [L].

p_j jth component of the vector of estimated parameters.

Q_{inj} injection rate [$L^3 T^{-1}$].

Q_{out} pumping rate [$L^3 T^{-1}$].

r radial coordinate (positive away from well) [L].

r_w well radius [L].

R_a retardation factor in the advective porosity [dimensionless].

R_d retardation factor in the diffusive porosity [dimensionless].

t time [T].

v pore water velocity [$L T^{-1}$].

V_p estimated parameter covariance matrix.

z coordinate along the diffusion pathway [L].

α_d diffusion rate coefficient (identically equivalent to D_a/l^2, see (2b)), which is continuously distributed in the multirate model [T^{-1}].

α_L the longitudinal dispersivity [L].

β_{tot} total capacity coefficient of the formation, which is the ratio of mass in the matrix to mass in the fractures at equilibrium [dimensionless].

$\delta(\alpha_d^*)$ Dirac delta (α_d^* represents a single value of α_d instead of a distribution) [T].

μ_d natural log of the geometric mean of the diffusion rate coefficients, ln [T^{-1}].

σ replicate variance defining the uncertainty in concentration.

σ_d standard deviation of the log-transformed diffusion rate coefficients, ln [T^{-1}].

σ_p standard deviation of the estimated parameter.

ϕ_a advective porosity [dimensionless].

ϕ_d diffusive porosity (equivalent to the matrix or "immobile zone" porosity) [dimensionless].

References

Altman, S. J., T. L. Jones, and L. C. Meigs, Controls on mass recovery for single-well injection-withdrawal tracer, in *Interpretations of Tracer Tests Performed in the Culebra Dolomite at the Waste Isolation Pilot Plant Site*, edited by L. C. Meigs, R. L. Beauheim, and T. L. Jones, *Rep. SAND97-3109*, chap. 4, pp. 37–68, Sandia Natl. Lab., Albuquerque, N. M., 2000.

Bahr, J. M., and J. Rubin, Direct comparison of kinetic and local equilibrium formulations for solute transport affected by surface reactions, *Water Resour. Res.*, 23(3), 438–452, 1987.

Ball, W. P., and P. V. Roberts, Long-term sorption of halogenated organic chemicals by aquifer material, 2, Intraparticle diffusion, *Environ. Sci. Technol.*, 25, 1237–1249, 1991.

Bard, Y., *Nonlinear Parameter Estimation*, Academic, San Diego, Calif., 1974.

Beauheim, R. L., and G. J. Ruskauff, Analysis of hydraulic tests of the Culebra and Magenta Dolomites and Dewey Lake Redbeds conducted at the Waste Isolation Pilot Plant Site, *Rep. SAND98-0049*, Sandia Natl. Lab., Albuquerque, N. M., 1998.

Brusseau, M. L., R. E. Jessup, and P. S. C. Rao, Modeling the transport of solutes influenced by multiprocess nonequilibrium, *Water Resour. Res.*, 25(9), 1971–1988, 1989.

Chen, W., and R. J. Wagenet, Solute transport in porous media with sorption-site heterogeneity, *Environ. Sci. Technol.*, 29, 2725–2734, 1995.

Chen, W., and R. J. Wagenet, Description of atrazine transport in soil with heterogeneous nonequilibrium sorption, *Soil Sci. Soc. Am. J.*, 61, 360–371, 1997.

Connaughton, D. F., J. R. Stedinger, L. W. Lion, and M. L. Shuler, Description of time-varying desorption kinetics: Release of napthalene from contaminated soils, *Environ. Sci. Technol.*, 27, 2397–2403, 1993.

Crank, J., *The Mathematics of Diffusion*, 2nd ed., Oxford Univ. Press, New York, 1975.

Culver, T. B., S. P. Hallisey, D. Sahoo, J. J. Deitsch, and J. A. Smith, Modeling the desorption of organic contaminants from long-term contaminated soil using distributed mass transfer rates, *Environ. Sci. Technol.*, 31(6), 1581–1588, 1997.

Cunningham, J. A., C. J. Werth, M. Reinhard, and P. V. Roberts, Effects of grain-scale mass transfer on the transport of volatile organics through sediments, 1, Model development, Water Resour. Res., 33(12), 2713–2726, 1997.

de Hoog, F. R., J. H. Knight, and A. N. Stokes, An improved method for numerical inversion of Laplace transforms, SIAM J. Sci. Comput., 3, 357–366, 1982.

Draper, N. R., and H. Smith, Applied Regression Analysis, 2nd ed., John Wiley, New York, 1981.

Fleming, S. W., Single and multiple rates of nonequilibrium diffusive mass transfer at the laboratory, field, and regional scales in the Culebra Member of the Rustler Formation, New Mexico, M.S. thesis, Oregon State Univ., Corvallis, 1998.

Fong, F. K., and L. A. Mulkey, Solute transport in aggregated media: Aggregated size distribution and mean radii, Water Resour. Res., 26(6), 1291–1303, 1990.

Gelhar, L. W., C. W. Welty, and K. R. Rehfeldt, A critical review of data on field-scale dispersion in aquifers, Water Resour. Res., 28(7), 1955–1974, 1992.

Goltz, M. N., and P. V. Roberts, Using the method of moments to analyze three-dimensional diffusion-limited solute transport from temporal and spatial perspectives, Water Resour. Res., 23(8), 1575–1585, 1987.

Hadermann, J., and W. Heer, The Grimsel (Switzerland) migration experiment: Integrating field experiments, laboratory investigations and modelling, J. Contam. Hydrol., 21, 87–100, 1996.

Haggerty, R., Laplace-domain solution for multirate model, in Interpretations of Tracer Tests Performed in the Culebra Dolomite at the Waste Isolation Pilot Plant Site, edited by L. C. Meigs, R. L. Beauheim, and T. L. Jones, Rep. SAND97-3109, Sandia Natl. Lab., Append. Q, pp. 351–353, Albuquerque, N. M., 2000.

Haggerty, R., and S. M. Gorelick, Multiple-rate mass transfer for modeling diffusion and surface reactions in media with pore-scale heterogeneity, Water Resour. Res., 31(10), 2383–2400, 1995.

Haggerty, R., and S. M. Gorelick, Modeling mass transfer processes in soil columns with pore-scale heterogeneity, Soil Sci. Soc. Am. J., 62(1), 62–74, 1998.

Haggerty, R., S. W. Fleming, and S. A. McKenna, STAMMT-R: Solute transport and multirate mass transfer in radial coordinates, Version 1.01, Rep. SAND99-0164, Sandia Natl. Lab., Albuquerque, N. M., 2000a.

Haggerty, R., S. A. McKenna, and L. C. Meigs, On the late-time behavior of tracer test breakthrough curves, Water Resour. Res., 36(12), 3467–3479, 2000b.

Harvey, C. F., R. Haggerty, and S. M. Gorelick, Aquifer remediation: A method for estimating mass transfer rate coefficients and an evaluation of pulsed pumping, Water Resour. Res., 30(7), 1979–1991, 1994.

Harvey, J. W., B. J. Wagner, and K. E. Bencala, Evaluating the reliability of the stream tracer approach to characterize stream-subsurface water exchange, Water Resour. Res., 32(8), 2441–2451, 1996.

Hollenbeck, K. J., C. F. Harvey, R. Haggerty, and C. J. Werth, A method for estimating distributions of mass transfer rate coefficients with application to purging and batch experiments, J. Contam. Hydrol., 37, 367–388, 1999.

Holt, R. M., Conceptual model for transport processes in the Culebra Dolomite Member, Rustler Formation, Rep. SAND97-0194, Sandia Natl. Lab., Albuquerque, N. M., 1997.

Kreft, A., and A. Zuber, Comments on "Flux-averaged and volume-averaged concentrations in continuum approaches to solute transport" by J. C. Parker and M. Th. van Genuchten, Water Resour. Res., 22(7), 1157–1158, 1986.

Lafolie, F., and C. Hayot, One-dimensional solute transport modelling in aggregated porous media, part 1, Model description and numerical solution, J. Hydrol., 143, 63–83, 1993.

Lessoff, S. C., and L. F. Konikow, Ambiguity in measuring matrix diffusion with single-well injection/recovery tracer tests, Ground Water, 35(1), 166–176, 1997.

Li, L., D. A. Barry, P. J. Culligan-Hensley, and K. Bajracharya, Mass transfer in soils with local stratification of hydraulic conductivity, Water Resour. Res., 30(11), 2891–2900, 1994.

Lorden, S. W., W. Chen, and L. W. Lion, Experiments and modeling of the transport of trichloroethene vapor in unsaturated aquifer material, Environ. Sci. Technol., 32(13), 2009–2017, 1998.

Marquardt, D., An algorithm for least-squares estimation of nonlinear parameters, SIAM J. Appl. Math., 11, 431–441, 1963.

McKenna, S. A., L. C. Meigs, and R. Haggerty, Tracer tests in a fractured dolomite, 3, Double-porosity, multiple-rate mass transfer processes in convergent-flow tracer tests, Water Resour. Res., this issue.

Meigs, L. C., and R. L. Beauheim, Tracer tests in a fractured dolomite, 1, Experimental design and observed tracer recoveries, Water Resour. Res., this issue.

Meigs, L. C., R. L. Beauheim, and T. L. Jones (Eds.), Interpretations of tracer tests performed in the Culebra Dolomite at the Waste Isolation Pilot Plant site, Rep. SAND97-3109, Sandia Natl. Lab., Albuquerque, N. M., 2000.

Neretnieks, I., Diffusion in the rock matrix: An important factor in radionuclide transport?, J. Geophys. Res., 85(B8), 4379–4397, 1980.

Neretnieks, I., Solute transport in fractured rock—Applications to radionuclide waste repositories, in Flow and Contaminant Transport in Fractured Rock, edited by J. Bear, C.-F. Tsant, and G. de Marsily, pp. 39–127, Academic, San Diego, Calif., 1993.

Pedit, J. A., and C. T. Miller, Heterogeneous sorption processes in subsurface systems, 1, Model formulations and applications, Environ. Sci. Technol., 28, 2094–2104, 1994.

Pedit, J. A., and C. T. Miller, Heterogeneous sorption processes in subsurface systems, 2, Diffusion modeling approaches, Environ. Sci. Technol., 29, 1766–1772, 1995.

Pignatello, J. J., and B. Xing, Mechanisms of slow sorption of organic chemicals to natural particles, Environ. Sci. Technol., 30, 1–11, 1996.

Quinodoz, H. A. M., and A. J. Valocchi, Stochastic analysis of the transport of kinetically sorbing solutes in aquifers with randomly heterogeneous hydraulic conductivity, Water Resour. Res., 29(9), 3227–3240, 1993.

Rao, P. S. C., D. E. Rolston, R. E. Jessup, and J. M. Davidson, Solute transport in aggregated porous media: Theoretical and experimental evaluation, Soil Sci. Soc. Am. J., 44, 1139–1146, 1980.

Rao, P. S. C., R. E. Jessup, and T. M. Addiscott, Experimental and theoretical aspects of solute diffusion in spherical and nonspherical aggregates, Soil Sci., 133(6), 342–349, 1982.

Rasmuson, A., The effect of particles of variable size, shape and properties on the dynamics of fixed beds, Chem. Eng. Sci., 40, 621–629, 1985.

Reeves, M., D. S. Ward, N. D. Johns, and R. M. Cranwell, Theory and implementation for SWIFT II, the Sandia Waste-Isolation Flow and Transport Model for fractured media release 4.84, Rep. SAND83-1159, NUREG/CR-3328, Sandia Natl. Lab., Albuquerque, N. M., 1986.

Ruthven, D. M., and K. F. Loughlin, The effect of crystallite shape and size distribution on diffusion measurements in molecular sieves, Chem. Eng. Sci., 26, 577–584, 1971.

Tidwell, V. C., L. C. Meigs, T. L. Christian-Frear, and C. M. Boney, Effects of spatially heterogeneous porosity on matrix diffusion as investigated by X-ray adsorption imaging, J. Contam. Hydrol., 42, 285–302, 2000.

Tsang, Y. W., Study of alternative tests in characterizing transport in fractured rocks, Geophys. Res. Lett., 22(11), 1421–1424, 1995.

Valocchi, A. J., Use of temporal moment analysis to study reactive solute transport in aggregated porous media, Geoderma, 46, 233–247, 1990.

van Genuchten, M. T., A general approach for modeling solute transport in structured soils, Mem. Int. Assoc. Hydrogeol., 17, 513–526, 1985.

Villermaux, J., Theory of linear chromatography, in Percolation Processes: Theory and Applications, NATO ASI Ser., Ser. E, vol. 33, edited by A. E. Rodrigues and D. Tondeur, pp. 83–140, Martinus Nijhoff, Zoetermeer, Netherlands, 1981.

Wagner, B. J., and J. W. Harvey, Experimental design for estimating parameters of rate-limited mass transfer: Analysis of stream tracer studies, Water Resour. Res., 33(7), 1731–1741, 1997.

Werth, C. J., J. A. Cunningham, P. V. Roberts, and M. Reinhard, Effects of grain-scale mass transfer on the transport of volatile organics through sediments, 2, Column results, Water Resour. Res., 33(12), 2727–2740, 1997.

Wu, S., and P. M. Gschwend, Numerical modeling of sorption kinetics of organic compounds to soil and sediment particles, Water Resour. Res., 24(8), 1373–1383, 1988.

S. W. Fleming, Waterstone Environmental Hydrology and Engineering, 1650 38th Street, Suite 201E, Boulder, CO 80301. (fleming_sean@hotmail.com)

R. Haggerty, Department of Geosciences, Oregon State University, 104 Wilkinson Hall, Corvallis, OR 97331-5506. (haggertr@ucs.orst.edu)

S. A. McKenna and L. C. Meigs, Geohydrology Department, Sandia National Laboratories, P.O. Box 5800, MS 0735, Albuquerque, NM 87185-0735. (samcken@sandia.gov; lcmeigs@sandia.gov)